Power Sub-Mesh Construction in Multiple Power Domain Design with IR Drop and Routability Optimization

Chien-Pang Lu
Intel Corporation
Hsinchu, Taiwan, ROC
knuth.lu@intel.com

Iris Hui-Ru Jiang
Graduate Institute of Electronics Engineering
National Taiwan University
Taipei, Taiwan, ROC
huirujiang@ntu.edu.tw

Chung-Ching Peng
Intel Corporation
Taipei, Taiwan, ROC
chung-ching.peng@intel.com

Mohd Razha Mohd Mawardi
Intel Corporation
Penang, Malaysia
mohd.mawardi.mohd.razha@intel.com

Uber Alessandro
Intel Corporation
Munich, Germany
alessandro.uber@intel.com

ABSTRACT

Multiple power domain design is prevalent for achieving aggressive power savings. In such design, power delivery to cross-domain cells poses a tough challenge at advanced technology nodes because of the stringent IR drop constraint and the routing resource competition between the secondary power routing and regular signal routing. Nevertheless, this challenge was rarely mentioned and studied in recent literature. Therefore, in this paper, we explore power sub-mesh construction to mitigate the IR drop issue for cross-domain cells and minimize its routing overhead. With the aid of physical, power, and timing related features, we train one IR drop prediction model and one design rule violation prediction model under power sub-meshes of various densities. The trained models effectively guide sub-mesh construction for cross-domain cells to budget the routing resource usage on secondary power routing and signal routing. Our experiments are conducted on industrial mobile designs manufactured by a 6nm process. Experimental results show that IR drop of cross-domain cells, the routing resource usage, and timing QoR are promising after our proposed methodology is applied.

CCS CONCEPTS

• **Hardware → Power grid design**.

KEYWORDS

Power grid, IR drop, routability, low power design.

ACM Reference Format:
Chien-Pang Lu, Iris Hui-Ru Jiang, Chung-Ching Peng, Mohd Razha Mohd Mawardi, and Uber Alessandro. 2024. Power Sub-Mesh Construction in Multiple Power Domain Design with IR Drop and Routability Optimization. In *Proceedings of the 2024 International Symposium on Physical Design (ISPD '24), March 12–15, 2024, Taipei, Taiwan.* ACM, New York, NY, USA, 8 pages. https://doi.org/10.1145/3626184.3633312

ISPD '24, March 12–15, 2024, Taipei, Taiwan

ACM ISBN 979-8-4007-0417-8/24/03.
https://doi.org/10.1145/3626184.3633312

1 INTRODUCTION

For achieving aggressive power savings, multiple power domains are prevalent in modern low power design. Power gating dynamically shuts off the power for an idle power domain, resulting in both static and dynamic power savings. In such design, a significant number of cells cross different domains, such as always-on buffers/inverters, retention flip-flops, isolation cells; each cross-domain cell should be connected to a proper power source to maintain functionality. Nevertheless, the routing between the secondary power pins on cross-domain cells and power sources compete with regular signal routing for the routing resource. As shown in Fig. 1(a), the primary power mesh occupies high layers, and high layer vias are relatively large at advanced technology nodes; thus, each of its stripes can offer a limited number of tapping vias. If a secondary power pin is not tapped to the nearest power stripe due to limited tapping vias or local congestion, it will take a long connection to a distant stripe and in turn induce a severe IR drop due to high resistance.

To resolve this problem, a local power sub-mesh can be constructed on lower layers as shown in Fig. 1(b), which provides smaller and more tapping vias, avoids long connections, and maintains low resistance. Moreover, cross-domain cells are irregularly distributed in a layout, as shown in Fig. 2(a); the power sub-mesh construction thus becomes nontrivial.

A full sub-mesh in Fig. 2(b) occupies excessive routing resource causing unwanted design rule violations on signal routing. A partial sub-mesh in Fig. 2(c), covering only the regions where cross-domain cells reside, can be further reduced if the distance to the available power source is taken into account as depicted in Fig. 2(d). Therefore, a careful arrangement for the sub-mesh density is of particular importance at advanced nodes to strike a balance between the IR drop of secondary power routing and design rule violations of signal routing.

Related works can be categorized into multiple power domain design techniques, IR drop prediction, power delivery network optimization, and routing hotspot prediction. Existing works on multiple power domain design techniques mainly focus on the wake-up signal routing/sequencing among power gating cells [17, 20] and buffering cross-domain cells [15, 16]. However, power delivery to cross-domain cells was rarely mentioned in literature. On the other

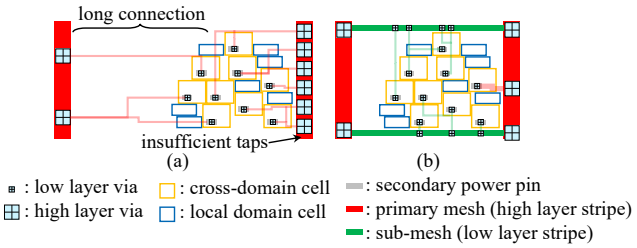

Figure 1: Cross-domain cells and secondary power routing in multiple power domain design at advanced process nodes.

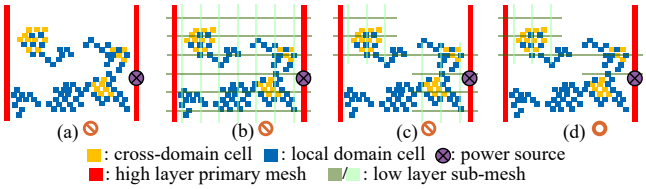

Figure 2: Power sub-mesh construction for reducing IR drop and routing overhead.

hand, recent research endeavors have been devoted to predicting IR drop by machine learning and using the prediction results to guide design ECO [4, 6–8, 10, 14, 22, 23]. Power mesh modification for IR drop optimization [5, 11, 12] or power mesh construction considering routability [3, 13] have been also investigated for primary power mesh. Recently, predicting design rule violations (also known as DRC hotspots) in a placed design has been extensively studied, e.g., [2, 9, 21]. However, these works mainly focus on primary power mesh construction and optimization, and prior DRC hotspot prediction models do not take the impact of routing secondary power pins into account.

Because there is not much research on power sub-mesh construction for cross-domain cells in recent literature, one possible solution can be derived, which starts with a full sub-mesh with the best IR drop (like Fig. 2(b)) and repeatedly removes unnecessary sub-meshes until the IR drop constraint cannot be satisfied any more. This iterative sub-mesh reduction approach requires time consuming IR drop analysis at each iteration, and possibly takes many iterations. To overcome the inefficiency, in this paper, by leveraging layout, power, and timing related features, we train one IR drop prediction model and one design rule violation prediction model under power sub-meshes of various densities. The trained models effectively guide sub-mesh construction for cross-domain cells to budget the routing resource usage on secondary power routing and signal routing. Meanwhile, we can mitigate the IR drop issue on cross-domain cells and minimize design rule violations incurred by signal routing simultaneously.

Our experiments are conducted on five industrial mobile designs manufactured by a 6nm process. Experimental results show that our models can accurately predict local IR drop and routing DRC hotspots, thus significantly reducing sub-mesh ECO iterations. Compared with the full sub-mesh strategy, the constructed power sub-meshes reduce the routing resource usage by up to 48% and decrease design rule violations by 60%, while satisfying a stringent 3% IR drop constraint and maintaining the same timing QoR. The proposed machine learning based dynamic power sub-mesh methodology is general and applicable to modern multiple domain designs, adopting sub-meshes mixed up with secondary power net routing for cross-domain cells.

The remainder of this paper is organized as follows. Section 2 briefly introduces power supply for cross-domain cells and describes the problem formulation. Section 3 details our dynamic power sub-mesh construction methodology. Section 4 shows experimental results on five industrial mobile designs. Finally, Section 5 concludes this work.

2 PRELIMINARIES

This section briefly introduces different types of power supplies to cross-domain cells and describes the problem formulation.

Power domain. In physical implementation, a typical power domain is a collection of cells located in a layout region that use the same power supply during normal operation and that can be switched on or off at the same time.

In a multiple power domain design, there are numerous cross-domain cells, e.g., always-on buffers/inverters, retention flip-flops, isolation cells. There are two types of power sources for a cross-domain cell:

Direct supply. The primary (constant) power mesh directly supplies power to a cross-domain cell.

Indirect supply. An indirect power source supplies power to a cross-domain cell. An indirect power source can be a power gating cell (MTCMOS) or a level shifter (in multiple supply voltage design).

Static IR drop. Static IR drop measures the weakness of overall power delivery network. Static IR drop can be estimated by

$$V_{static\_drop} = I_{avg} \times R_{wire},$$

where I_{avg} denotes the average current drawn from the power delivery network under an average switching condition, and R_{wire} denotes the effective resistance from the power source to a location of interest in a layout. The increased resistance and current density coming with device scaling create a reliability concern.

The connection between the power source and the secondary power pin of a cross-domain cell is usually routed by wider metals (set by nondefault routing rules) than signal routing. Even so, a long connection still may incur an IR drop violation due to high resistance. As mentioned earlier, a power sub-mesh can be constructed below the primary power mesh using low layer metals. Such mesh structure reduces the wire resistance and in turn lowers the IR drop value, and it provides more via tapping locations to resolve the long connection issue. According to the IR drop and current analysis reported by a commercial tool [1], Fig. 3(a) shows the local IR drop can be reduced after power sub-mesh deployment. Concurrently, it increases the current for the local cross-domain cells as shown in Fig. 3(b).

Therefore, in this paper, we address the power sub-mesh deployment problem for cross-domain cells as follows:

Problem: Given a timing-driven placed and clock-routed multiple power domain design, a set of cross-domain cells and corresponding power sources, primary power mesh and signal routing

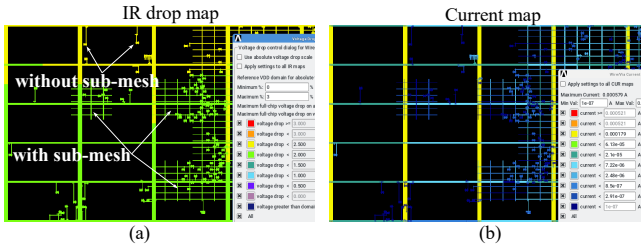

Figure 3: Cross-domain cells with/without power sub-meshes. (a) Static IR drop distribution. (b) Current distribution.

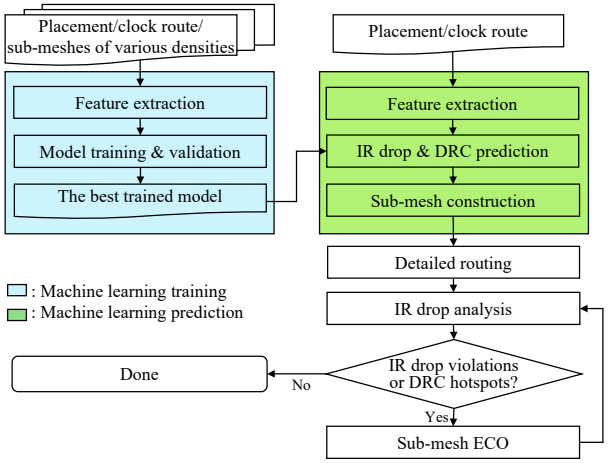

Figure 4: Overall flow of our power sub-mesh construction methodology.

distributions, our goal is to construct power sub-meshes such that the IR drop constraints on cross-domain cells are satisfied, the design rule violations on signal routing are minimized without timing degradation.

3 DYNAMIC POWER SUB-MESH CONSTRUCTION

This section details our power sub-mesh construction approach.

3.1 Overview

Fig. 4 shows the overall flow of our methodology. Given the placement and clock route of a multiple power domain design, sub-meshes are dynamically constructed according to cross-domain cell locations, primary power mesh and signal routing distributions. Then, IR drop analysis performs after detailed routing. If there are IR drop violations or design rule violations, the density of sub-meshes with violations will be locally increased or decreased; the sub-mesh ECO and IR drop analysis are iterated until no improvement.

Because IR drop analysis is time consuming, constructing a proper power sub-mesh is desired to minimize sub-mesh ECO runs. In this work, with the aid of physical, power, and timing related features, we train one IR drop prediction model and one design rule violation prediction model under power sub-meshes of various densities. The trained models effectively guide sub-mesh construction for cross-domain cells to balance the routing resource usage on secondary power routing and signal routing. Meanwhile, we can mitigate the IR drop issue on cross-domain cells and minimize design rule violations incurred by signal routing simultaneously. Our results will show that our models are accurate, and sub-mesh ECO can thus possibly avoided.

3.2 Feature Extraction

Feature engineering plays an important role for generating accurate static IR drop and DRC hotspot predictions. First of all, training layouts are generated by a multiple power domain design with different densities of sub-meshes. Then, each training layout is partitioned into uniform grids; the grid size is properly set according to primary power mesh structure, the distribution of cross-domain cells and the distribution of signal and clock routing. For each target cell (cross-domain cell), features are collected with respect to its corresponding layout grid.

Table 1 lists all features that we consider in this paper to predict static IR drop and DRC hotspots. For a cross-domain cell, we extract the following features: SMD_j and RMD_j represents the layer-specific power/ground metal density of sub-mesh and that of primary power mesh over a grid of interest, respectively. SMD_j (RMD_j) is collected for each layer j where the sub-mesh (primary mesh) occupies. The metal density is computed by the ratio of the corresponding metal area on the specific layer to the grid area. The following area density, output loading density, and signal routing density features are computed in a similar way. SD_j means signal routing density at each layer j over a grid of interest. The signal routing shapes are extracted from the global routing done by a physical synthesis tool. CA, CL and CP are the area, output loading, and clock period of the target cell. $NNAD$ and $NNLD$ are the area density and output loading density of the neighboring cells in the same grid and supplied by the same constant power on N-well. $NSAD$ and $NSLD$ are the area density and output loading density of the neighboring cells in the same grid and connected to the same secondary power source. $PGSD$ is the distance from the target cell to the primary power mesh. PGD is the distance from the target cell to the corresponding power source.

These features can be classified into three categories: physical, power and timing features, so that we can simulate I_{avg}, R_{wire} and routing congestion information. Physical features can further divided into resistance related features, SMD_j, RMD_j, CA, and congestion related features, SD_j, $NNLD$ and $NSLD$. Power features include the target cell's $NNAD$, $NSAD$, $PGSD$ and PGD. Finally, timing features include the target cell's CL and CP. In our experiments, we will extract 46 features for each target cell.

Furthermore, in the training phase, we collect two target variables: 1) the static IR drop value of each cross-domain cell (with direct or indirect supply) reported by the IR drop simulation tool, 2) DRC hotspot grids from detailed routing.

Table 1: Features Classified into Physical, Power, and Timing Categories.

Physical	Power	Timing	Features	Description
✓R			SMD_j	Sub-mesh power/ground metal density on layer j over a grid.
✓R			RMD_j	Primary mesh power/ground metal density on layer j over a grid.
✓C			SD_j	Signal routing density on layer j over a grid.
✓R			CA	Area of target cell.
		✓	CL	Loading of target cell (i.e. total output loading).
		✓	CP	Clock period of target cell (extracted from timing report).
	✓		$NNAD$	Area density of neighboring cells (supplied by the same constant power on N-well) over a grid.
	✓		$NSAD$	Area density of neighboring cells (supplied by the same power on their secondary power pins) over a grid.
✓C			$NNLD$	Loading density of neighboring cells (supplied by the same constant power on N-well) over a grid.
✓C			$NSLD$	Loading density of neighboring cells (supplied by the same power on their secondary power pins) over a grid.
	✓		$PGSD$	The distance from target cell to power/ground source.
	✓		PGD	The distance from target cell to indirect power source (power gating cell, level shifter).

*R: resistance related features; C: congestion related features.

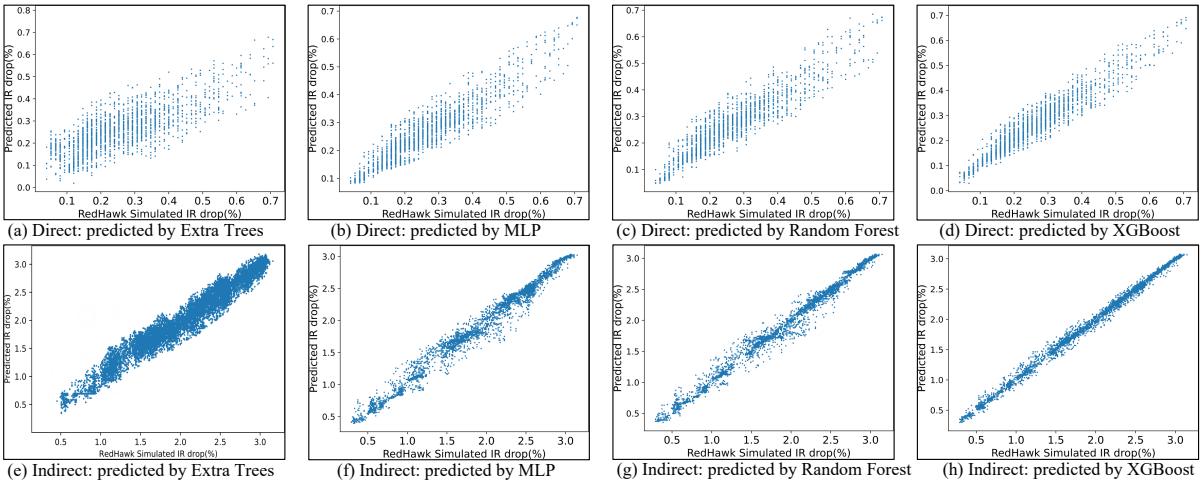

(a) Direct: predicted by Extra Trees (b) Direct: predicted by MLP (c) Direct: predicted by Random Forest (d) Direct: predicted by XGBoost

(e) Indirect: predicted by Extra Trees (f) Indirect: predicted by MLP (g) Indirect: predicted by Random Forest (h) Indirect: predicted by XGBoost

Figure 5: Different regression models on IR drop percentage prediction for cross-domain cells with direct and indirect supplies in an industrial design ckt1.

Table 2: Performance achieved by different regression models: Extra Trees, MLP, Random Forest, and XGBoost.

Model	*MAE* (Direct/Indirect/DRC)	*RMSE* (Direct/Indirect/DRC)	R^2 score (Direct/Indirect/DRC)	*C.C.* (Direct/Indirect/DRC)
Extra Trees	0.07 / 0.24 / 0.35	0.09 / 0.30 / 0.23	0.57 / 0.83 / 0.73	0.73 / 0.91 / 0.77
MLP	0.04 / 0.08 / 0.31	0.06 / 0.12 / 0.16	0.84 / 0.97 / 0.71	0.91 / 0.97 / 0.72
Random Forest	0.04 / 0.06 / 0.12	0.06 / 0.12 / 0.13	0.84 / 0.98 / 0.82	0.91 / 0.99 / 0.83
XGBoost	0.03 / 0.04 / 0.11	0.05 / 0.09 / 0.13	0.91 / 0.99 / 0.81	0.94 / 0.99 / 0.81

3.3 Machine Learning Models

Two datasets are adopted to train machine learning models, D^{ir} for IR drop percentage prediction of a given cell instance and D^{drc} for the DRC hotspot prediction for the grid where the cell is located.

- $D^{ir} = \{(x_i, \hat{y}_i^{ir})\}, |D^{ir}| = N, x_i \in R^n, \hat{y}_i^{ir} \in R.$
- $D^{drc} = \{(x_i, \hat{y}_i^{drc})\}, |D^{drc}| = N, x_i \in R^n, \hat{y}_i^{drc} \in \{0, 1\}.$

Based on the feature extraction in the previous subsection, x_i is the feature set of the i-th target cell instance, N is the total number of the cells, and n is the feature dimension. $\hat{y}_i^{ir}$ is the IR drop percentage value of cell i provided by static IR drop analysis. $\hat{y}_i^{drc}$ indicates if there is a DRC hotspot at the grid containing cell i. We extract these features from the training layouts with sub-meshes of various densities; in our experiments, the datasets contain around 20K cross-domain cell instances, and split them into training and validation sets with 80 : 20 split ratio. Moreover, for facilitating model training, we perform normalization and standardization on the data feature values before the training process.

We train multiple regression models and output the model with the best prediction performance on the validation set for the subsequent inference on test layouts.

Extra Trees are an ensemble learning method that combines the decisions from multiple decision trees. Instead of calculating a locally optimal value, it randomly selects a split value from the x_i features, making the trees diversified and uncorrelated.

MLP (ANN) is a misnomer for a modern feedforward artificial neural network and consists of multiple layers of interconnected neurons, which are organized into an input layer, one or more hidden layers, and an output layer. Each layer is represented as $y = f(Wx^T + b)$, where f is the activation function, W is the set

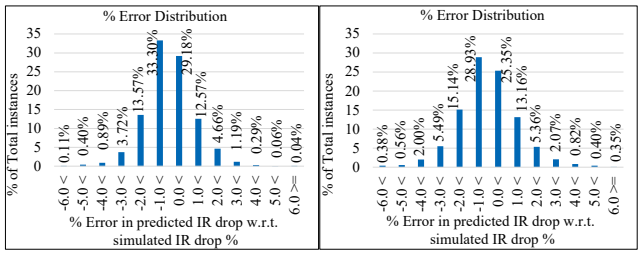

Figure 6: % Error distribution of XGBoost for cross-domain cells with (a) direct supply and (b) indirect supply.

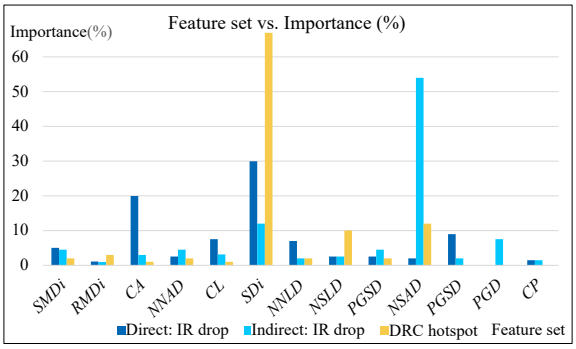

Figure 7: Feature importance reported by XGBoost.

of weights in the layers, x is the input vector, and b is the bias vector. We use ReLU (Rectified Linear Unit) and softmax activation functions.

Random Forest is commonly used for a wide range of machine learning tasks. It constructs an uncorrelated forest of decision trees by recursively splitting the data based on random subset of the x_i features. The individual decision trees will be averaged or perform a majority vote to finalize the prediction.

XGBoost is a distributed gradient boosting regression tree. It ensembles multiple additive functions as regression trees to obtain the output y_i, and $y_i = \phi(x_i) = \sum_{k=1}^{K} f_k(x_i), f_k \in F$, where F is the space of K addictive functions.

According to the validation results, the best model trained by XGBoost is selected. In the following, Table 2, Fig. 5, Fig. 6, and Fig. 7 show model evaluation results on a test layout (industrial mobile design ckt1). Table 2 compares the performance of each regression model on mean absolute error (*MAE*), root mean square error (*RMSE*), R-squared (R^2) and correlation coefficient (*C.C.*), where 'Direct' indicates the result of IR drop on cross-domain cells with direct supply; 'Indirect' IR drop on cross-domain cells with indirect supply; 'DRC' DRC hotspot in a grid. Fig. 5 show the correlation between the predicted IR drop percentage and the simulated IR drop percentage. The working voltage is 0.75V for direct and indirect supply. The first row shows the results of cross-domain cells with direct supply, while the second row for indirect supply. It can be seen that the RMSE, R^2 score, and correlation of XGBoost is obviously superior to Extra Trees, MLP, and Random Forest thus being selected as the best trained model. In addition, Fig. 6 shows the histogram of % error distribution of XGBoost; Fig. 7 illustrates the importance of each feature by using XGBoost on the multi-task training, IR drop of cross-domain cells with direct and indirect supplies and DRC hotspots.

Overall, the results show that our features can capture the behavior of IR drop and DRC hotspots well, and thus simple machine learning models can deliver accurate predictions.

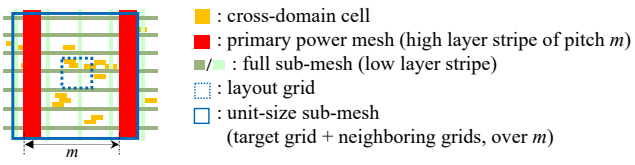

Figure 8: Layout grid size and the unit size of sub-meshes.

3.4 Unit Size Selection for Sub-Meshes

The unit size of sub-mesh determines the search range for extracting features of neighboring cells. As shown in Fig. 8, a unit size of sub-mesh should overlap with the primary power mesh so that it can receive supply; the unit size can contain more than one layout grid. Take a sample design manufactured by 6nm process as an example; considering a layout grid of size 1x1 nm^2, Fig. 9(a) and (b) shows the area density of neighboring cells and signal routing density within each layout grid, respectively. When the search range covers more than one layout grid, the densities collected in each grid as shown in Fig. 9(a) will be further merged as features. Fig. 9(c) shows the R^2 score and runtime under different search ranges (in terms of one layout grid of the target cross-domain cell plus several neighboring grids). The larger search range, the longer runtime for collecting the information of neighboring cells. When the unit size of sub-meshes exceeds 5x5 grids, the unit size is wider than the pitch of primary power mesh; when the unit size exceeds 6x6 grids, R^2 score is above 0.99. For this setting, the unit size of sub-meshes is chosen to be 6x6 grids.

3.5 Model Prediction and ECO Selection

The main purpose of sub-mesh construction is maintaining IR drop and reducing DRC hotspots. As shown in Fig. 4, all cells in a test layout are legalized; clock routing and global routing (signal routing distributions) are done by a commercial tool at timing-driven mode [19].

First, all features of each cross-domain cell in the test layout are extracted. In particular, a set of different settings of SMD_i, reflecting sub-meshes of various densities, are applied during the model inference. Hence, the corresponding set of IR drop values on each cross-domain cell (with either direct or indirect supply) and DRC hotspot flags (0/1 indicates without/with DRC hotspot) are obtained. Then, the smallest SMD_i setting that meets the IR drop constraint and has no DRC hotspot will be the sub-mesh configuration for the grid where the cross-domain cell is located. If no SMD_i setting meets both requirements, then the grid will

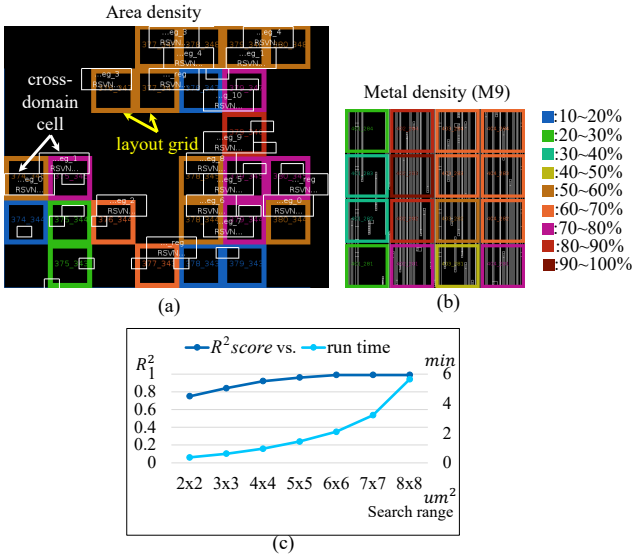

Figure 9: Unit size selection for sub-meshses. (a) Area density of neighboring cells within each layout grid. (b) Signal routing density on a specific layer of each layout grid. (c) R^2 and runtime of extraction and merging neighboring grids.

be skipped and handled by ECO. The IR drop constraint used in inference is usually smaller than the actual constraint.

4 EXPERIMENTAL RESULTS

We implemented our approach in the C++, Tcl and Python 3.7.4 (scikit-learn package) language on an Intel Xeon Linux workstation with 3.2 GHz CPU and 512 GB memory. Table 3 lists benchmark statistics, including five industrial mobile designs with 6nm process. 'CKT' denotes design, '# of Cells' denotes the number of all cell instances in a design, '# of Domains' the number of power domains, 'Area' the total standard cell area, '# of Nets' the number of nets, '# of Direct' the number of cross-domain cell instances with direct supply, '# of Indirect' the number of cross-domain cell instances with indirect supply, 'Period' the smallest clock period in a design. In our experiments, all designs are placed at timing optimization mode by a commercial tool [19], timing is reported by [18], and IR drop analysis is done by [1]. For these benchmark circuits, the primary power mesh is constructed on metal 10 and metal 11 layers, and sub-meshes are on metal 8 and metal 9 layers. The IR drop constraint is 3% of the working voltage. One sample design with 2 power domains and 20k cross-domain cells is used to generate the training datasets.

Table 4 compares our machine learning approach (ML) trained by XGBoost with no sub-mesh (None), full sub-mesh (Full) and global route congestion-aware sub-mesh (GR-aware). When no sub-meshes are constructed, the power delivery to secondary power pins on cross-domain cells is done by nondefault routing. Because the sub-mesh competes over the routing resource with signal routing, the global route congestion-aware method constructs sub-meshes only when the average layer-wise routing density is under 40%. For

Table 3: Benchmark Statistics.

CKT.	# of Cells	# of Domains	Area (um^2)	# of Nets	# of Direct	# of Indirect	Period (ns)
ckt1	940329	2	258567	4167119	10000	17921	0.312
ckt2	620610	2	937054	875909	31708	1629	0.312
ckt3	557635	4	365361	13060997	5438	9609	0.312
ckt4	1075600	2	328038	1651630	3414	11695	0.312
ckt5	225094	6	322605	367503	2204	4819	0.500

our ML approach, during inference, we set a more conservative IR drop constraint, where the predicted static IR drop should be less than 1%, and there are zero DRC hotspots for each sub-mesh unit. After sub-mesh construction, we complete physical design flow by commercial tools and report the following statistics according to the detailed routing results generated by the the three methodologies. 'Sub-mesh length' denotes the total sub-mesh length, 'Sub-mesh coverage% (Direct / Indirect)' denotes the ratio of sub-mesh coverage with respect to the grids where cross-domain cells (with direct/indirect supply) are located, 'Direct IR% (max/avg)' denotes the maximum and average IR drop percentage of cross-domain cells with direct supply, 'Indirect IR% (max/avg)' denotes the maximum and average IR drop percentage of cross-domain cells with indirect supply, 'IR Improved Cells%' denotes the percentage of cross-domain cells whose IR drop is improved by ML, '# of over 3% IR Cells' denotes the number of cross-domain cells whose IR drop exceed the 3% IR drop constraint, '# of DRCs' denotes the number of design rule violations in a design, and 'Runtime' denotes the run time, but not including the time of running commercial tools. In addition, 'ML*' indicates that some of sub-meshes use double stripes in the design.

Overall, our approach outperforms no sub-mesh, full sub-mesh and GR congestion aware methodologies. For each design, our approach cleans all IR drop violations on cross-domain cells and result in the fewest DRC hotspots. Compared with full sub-mesh, our method cleans all IR drop violations by utilizing much shorter (51.5%) sub-mesh length. Compared with the GR congestion aware method, our method significantly reduces DRC violations. The reason is our method dynamically determines the density of each sub-mesh according to the physical, power, and timing features of the target grid. In addition, the timing remains almost the same (less than 5 picoseconds difference) in all cases (in terms of worst negative slack and total negative slack in setup and hold timing). Fig. 10 compares the IR drop distribution by applying our ML approach with no sub-mesh. Fig. 11(a) shows the no sub-mesh method results in 8 routing shorts in design 'ck3', while Fig. 11(b) shows no short issue incurred by our method in the same layout region. This result shows that our ML approach can strike a balance between IR drop optimization and routability especially for congested regions. The IR drop experienced by a cross-domain cell with direct supply is usually lower than that with indirect supply because the primary power mesh has a higher density. Fig. 12 shows the power sub-mesh produced by our method. By considering the distance to the power source and modeling the IR drop impact, our method appropriately decreases the sub-mesh usage for cross-domain cells with direct supply and reserves more routing resource for the sub-mesh of cross-domain cells with indirect supply. The time spent on

Table 4: Comparison Results of No Sub-mesh (None), Full Sub-mesh (Full), Global Route Congestion-aware Sub-mesh (GR-aware) and Our Machine Learning Approach (ML).

CKT	Methodology	Sub-mesh length (um)	Sub-mesh coverage% (Direct / Indirect)	Direct IR% (max / avg)	Indirect IR% (max / avg)	IR Improved Cells%	# of over 3% IR Cells	# of DRCs	Runtime (sec)
ckt1	None	0	0.0 / 0.0	1.641 / 0.313	3.052 / 1.819	89.32	627	56	-
	Full	314459	100.0 / 100.0	1.275 / 0.300	2.991 / 1.801	2.26	0	43	15
	GR-aware	29308	87.4 / 94.4	1.405 / 0.306	2.991 / 1.804	9.23	0	40	193
	Ours: ML*	130501	0.2 / 94.5	1.640 / 0.313	2.987 / 1.799	-	0	20	198
ckt2	None	0	0.0 / 0.0	2.280 / 0.422	3.096 / 0.818	93.50	32	182	-
	Full	1955527	100.0 / 100.0	1.720 / 0.406	3.004 / 0.786	0.07	2	52	8
	GR-aware	1682633	82.5 / 89.9	1.735 / 0.420	3.010 / 0.803	5.48	2	41	218
	Ours: ML*	1243836	29.8 / 95.2	1.782 / 0.420	2.979 / 0.800	-	0	16	206
ckt3	None	0	0.0 / 0.0	0.990 / 0.187	1.604 / 0.538	13.59	0	197	-
	Full	79325	100.0 / 100.0	0.987 / 0.181	1.600 / 0.545	0	0	163	10
	GR-aware	69382	80.9 / 77.5	0.987 / 0.184	1.600 / 0.545	3.68	0	109	392
	Ours: ML	41121	16.3 / 99.2	0.996 / 0.183	1.600 / 0.545	-	0	60	401
ckt4	None	0	0.0 / 0.0	0.907 / 0.050	1.000 / 0.332	98.44	0	446	-
	Full	912931	100.0 / 100.0	0.890 / 0.049	0.733 / 0.293	0	0	83	18
	GR-aware	698389	78.2 / 74.5	0.890 / 0.049	0.733 / 0.299	5.71	0	85	212
	Ours: ML	294302	3.50 / 99.8	0.893 / 0.050	0.734 / 0.299	-	0	33	207
ckt5	None	0	0.0 / 0.0	0.827 / 0.108	3.080 / 1.081	26.96	97	41	-
	Full	173684	100.0 / 100.0	0.772 / 0.103	2.792 / 1.065	22.21	0	58	8
	GR-aware	146283	85.2 / 81.5	0.793 / 0.105	2.842 / 1.071	14.23	0	58	163
	Ours: ML*	62425	1.100 / 51.6	0.812 / 0.110	2.740 / 1.071	-	0	33	167
Ratio	None	0	0.0 / 0.0	1.177 / 1.039	1.063 / 1.020	13.113	378.000	1.817	-
	Full	1.000	1.000 / 1.000	1.000 / 1.000	1.000 / 1.000	1.000	1.000	1.000	1.000
	GR-aware	0.841	0.828 / 0.835	1.029 / 1.024	1.004 / 1.007	1.561	1.000	0.834	19.966
	Ours: ML	0.515	0.101 / 0.880	1.084 / 1.035	0.992 / 1.004	-	0	0.406	19.983

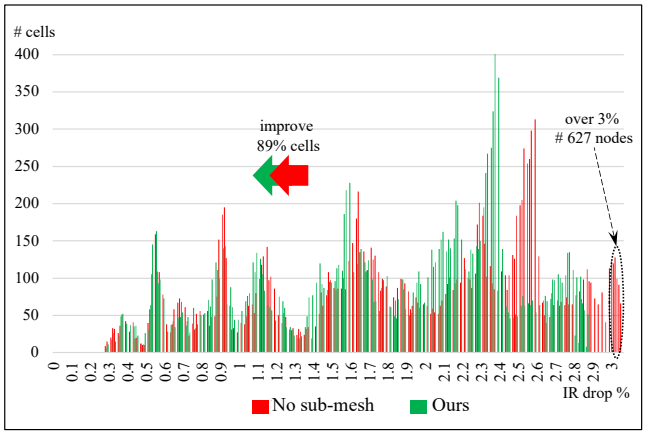

Figure 10: No sub-mesh vs. our ML approach for ckt1.

placement, routing, and IR drop analysis tools [1, 19] ranges from more than ten to tens of hours. Specifically, IR drop analysis takes around 1 to 1.5 hours for each case. The runtime of our approach taken on feature extraction, IR drop and DRC prediction, sub-mesh construction, and sub-mesh ECO ranges from 167 to 401 seconds. In particular, sub-mesh construction takes only several seconds. Thus, the runtime overhead can be omitted compared with the the time spent on commercial tools. Hence, it can be seen that our methodology can effectively reduce IR drop and DRC fixing iterations and is promising to be incorporated into the practical physical design flow.

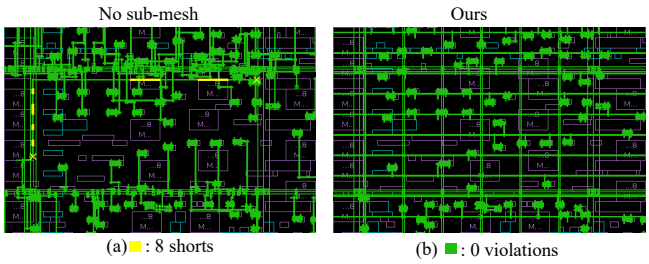

Figure 11: Partial layout of ckt3. (a) No sub-mesh: 8 shorts. (b) Ours: 0 shorts.

5 CONCLUSION

The stringent IR drop constraint and the routing resource competition between the secondary power routing and regular signal routing make power delivery to cross-domain cells challenging in multple power domain design. In this paper, we propose a machine learning based power sub-mesh construction methodology. With the aid of physical, power, and timing related features, the trained models can capture the behaviors of IR drop and DRC hotspots well. Experimental results show that IR drop of cross-domain cells, the routing resource usage, and timing QoR are promising after our proposed methodology is applied. Future work includes incorporating end-to-end machine learning models and extension to dynamic IR drop optimization.

REFERENCES

[1] Ansys, Inc. 2020. RedHawk, version 2020 R1.4p5 RHEL6. https://www.ansys.com/

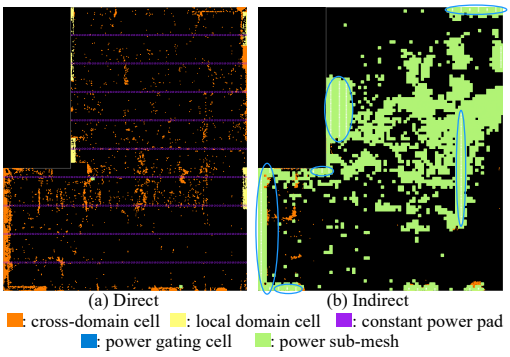

Figure 12: Power sub-mesh for ckt1 generated by our method.

[2] K. Baek, H. Park, S. Kim, K. Choi, and Taewhan Kim. 2022. Pin Accessibility and Routing Congestion Aware DRC Hotspot Prediction Using Graph Neural Network and U-Net. In *Proceedings of International Conference on Computer-Aided Design (ICCAD)*. IEEE, San Diego, California, Article 26, 9 pages. https://ieeexplore.ieee.org/stamp/stamp.jsp?tp=&arnumber=10070024

[3] W.-H. Chang, C.-H. Lin, S.-P. Mu, L.-D. Chen, C.-H. Tsai, Y.-C. Chiu, and Mango C.-T. Chao. 2017. Generating Routing-Driven Power Distribution Networks With Machine-Learning Technique. *IEEE Transactions on Computer-Aided Design of Integrated Circuits and Systems* 36 (2017), 1237–1250. https://doi.org/10.1109/TCAD.2017.2648842

[4] Y.-C. Fang, H.-Y. Lin, M.-Y. Su, C.-M. Li, and Eric J.-W. Fang. 2018. Machine-learning-based Dynamic IR Drop Prediction for ECO. In *Proceedings of International Conference on Computer-Aided Design (ICCAD)*. IEEE, San Diego, CA, 7 pages. https://ieeexplore.ieee.org/stamp/stamp.jsp?tp=&arnumber=8587752

[5] S.-I. Heo, Andre B. Kahng, M. Kim, L. Wang, and C. Yang. 2019. Detailed Placement for IR Drop Mitigation by Power Staple Insertion in Sub-10nm VLSI. In *Proceedings of Design, Automation and Test in Europe Conference (DATE)*. IEEE, Florence, Italy, 6 pages. https://ieeexplore.ieee.org/stamp/stamp.jsp?tp=&arnumber=8715096

[6] C.-T. Ho and Andrew B. Kahng. 2019. IncPIRD: Fast Learning-Based Prediction of Incremental IR Drop. In *Proceedings of International Conference on Computer-Aided Design (ICCAD)*. IEEE, Westminster, CO, 8 pages. https://ieeexplore.ieee.org/stamp/stamp.jsp?tp=&arnumber=8942110

[7] X.-X. Huang, H.-C. Chen, S.-W. Wang, I. H.-R. Jiang, Y.-C. Chou, and C.-H. Tsai. 2020. Dynamic IR-Drop ECO Optimization by Cell Movement with Current Waveform Staggering and Machine Learning Guidance. In *Proceedings of International Conference On Computer Aided Design (ICCAD)*. IEEE, San Diego, CA, 9 pages. https://ieeexplore.ieee.org/stamp/stamp.jsp?tp=&arnumber=9256574

[8] S. Kundu, M. Prasad, S. Nishad, S. Nachireddy, and H. K. 2022. MLIR: Machine Learning based IR Drop Prediction on ECO Revised Design for Faster Convergence. In *Proceedings of International Conference on VLSI Design International Conference on Embedded Systems (VLSID)*. IEEE, Bangalore, India, 6 pages. https://ieeexplore.ieee.org/stamp/stamp.jsp?tp=&arnumber=9885875

[9] R. Liang, H. Xiang, D. Pandey, L. Reddy, S. Ramji, G.-J. Nam, and J. Hu. 2020. DRC Hotspot Prediction at Sub-10nm Process Nodes Using Customized Convolutional Network. In *Proceedings of International Symposium on Physical Design (ISPD)*. ACM, Taipei, Taiwan, 135–142. https://dl.acm.org/doi/pdf/10.1145/3372780.3375560

[10] H.-Y. Lin, Y.-C. Fang, S.-T. Liu, J.-X. Chen, C.-M. Li, and Eric J.W. Fang. 2020. Automatic IR-Drop ECO Using Machine Learning. In *Proceedings of International Test Conference in Asia (ITC-Asia)*. IEEE, Taipei, Taiwan, 6 pages. https://ieeexplore.ieee.org/stamp/stamp.jsp?tp=&arnumber=9226557

[11] J.-M. Lin, Y.-T. Chen, Y.-T. Kung, and H.-J. Lin. 2023. Voltage-Drop Optimization Through Insertion of Extra Stripes to a Power Delivery Network. In *Proceedings of International Symposium on Physical Design (ISPD)*. ACM, Virtual Event, USA, 35–43. https://dl.acm.org/doi/pdf/10.1145/3569052.3571870

[12] J.-M. Lin, Y.-T. Kung, Z.-Y. Huang, and I.-R. Chen. 2021. A Fast Power Network Optimization Algorithm for Improving Dynamic IR-Drop. In *Proceedings of International Symposium on Physical Design (ISPD)*. ACM, Virtual Event, USA, 91–98. https://dl.acm.org/doi/pdf/10.1145/3439706.3447042

[13] J.-M. Lin, J.-S. Syu, and I.-R. Chen. 2018. Macro-Aware Row-Style Power Delivery Network Design for Better Routability. In *Proceedings of International Conference on Computer-Aided Design (ICCAD)*. IEEE, San Diego, CA, 8 pages. https://ieeexplore.ieee.org/stamp/stamp.jsp?tp=&arnumber=8587733

[14] S.-Y. Lin, Y.-C. Li, Y.-C. Liu, T.-S. Yang, S.-C. Lin, C.-M. Li, and Eric J.W. Fang. 2018. IR drop prediction of ECO-revised circuits using machine learning. In *Proceedings of VLSI Test Symposium (VTS)*. IEEE, San Francisco, CA, 6 pages. https://ieeexplore.ieee.org/stamp/stamp.jsp?tp=&arnumber=8368657

[15] C.-P. Lu and I. H.-R. Jiang. 2018. COSAT: Congestion, Obstacle, and Slew Aware Tree Construction for Multiple Power Domain Design. In *Proceedings of Design Automation Conference (DAC)*. IEEE, San Francisco, CA, 6 pages. https://ieeexplore.ieee.org/stamp/stamp.jsp?tp=&arnumber=8465899

[16] C.-P. Lu, I. H.-R. Jiang, and C.-H. Hsu. 2015. GasStation: Power and area efficient buffering for multiple power domain design. In *Proceedings of International Conference on Computer-Aided Design (ICCAD)*. IEEE, Austin, TX, 861–866. https://doi.org/10.1109/ICCAD.2015.7372661

[17] Y.-T. Shyu, J.-M. Lin, C.-C. Lin, C.-P. Huang, and S.-J. Chang. 2016. An Efficient and Effective Methodology to Control Turn-On Sequence of Power Switches for Power Gating Designs. *Proceedings of IEEE Transactions on Computer-Aided Design of Integrated Circuits and Systems (TCAD)* 35 (2016), 1730–1743. https://doi.org/10.1109/TCAD.2016.2523916

[18] Synopsys, Inc. 2020. PrimeTime, version R-2020.09-SP3. https://www.synopsys.com/

[19] Synopsys, Inc. 2021. Fushion Compiler, version S-2021.06-SP5. https://www.synopsys.com/

[20] T.-M. Tseng, Mango C.-T. Chao, C.-P. Lu, and C.-H. Lo. 2009. Power-switch routing for coarse-grain MTCMOS technologies. In *Proceedings of International Conference on Computer-Aided Design (ICCAD)*. IEEE, San Jose, CA, 39–46. https://ieeexplore.ieee.org/stamp/stamp.jsp?tp=&arnumber=5361318

[21] Z. Xie, Y.-H. Huang, G.-Q. Fang, H. Ren, S.-Y. Fang, Y. Chen, and J. Hu. 2018. RouteNet: Routability Prediction for Mixed-Size Designs Using Convolutional Neural Network. In *Proceedings of International Conference on Computer-Aided Design (ICCAD)*. IEEE, San Diego, CA, 8 pages. https://doi.org/10.1145/3240765.3240843

[22] Z. Xie, H. Ren, B. Khailany, Y. Sheng, S. Santosh, J. Hu, and Y. Chen. 2020. PowerNet: Transferable Dynamic IR Drop Estimation via Maximum Convolutional Neural Network. In *Proceedings of Asia and South Pacific Design Automation Conference (ASP-DAC)*. IEEE, Beijing, China, 6 pages. https://ieeexplore.ieee.org/stamp/stamp.jsp?tp=&arnumber=9045574

[23] F. Ye, F. Firouzi, Y. Yang, K. Chakrabarty, and M.-B. Tahoori. 2014. On-Chip Voltage-Droop Prediction Using Support-Vector Machines. In *Proceedings of VLSI Test Symposium (VTS)*. IEEE, Napa, CA, 6 pages. https://ieeexplore.ieee.org/stamp/stamp.jsp?tp=&arnumber=6818798